Journal Pre-proof

Diagnostic Accuracy of Wide-Field Map from Swept-Source Optical Coherence Tomography for Primary Open-Angle Glaucoma in Myopic Eyes

Yong Woo Kim, Jinho Lee, Jin-Soo Kim, Ki Ho Park

PII: S0002-9394(20)30273-7

DOI: https://doi.org/10.1016/j.ajo.2020.05.032

Reference: AJOPHT 11385

To appear in: *American Journal of Ophthalmology*

Received Date: 15 March 2020

Revised Date: 25 May 2020

Accepted Date: 25 May 2020

Please cite this article as: Kim YW, Lee J, Kim J-S, Park KH, Diagnostic Accuracy of Wide-Field Map from Swept-Source Optical Coherence Tomography for Primary Open-Angle Glaucoma in Myopic Eyes, *American Journal of Ophthalmology* (2020), doi: https://doi.org/10.1016/j.ajo.2020.05.032.

ABSTRACT

Purpose: To compare the accuracy for glaucomatous defects and diagnostic power for primary open-angle glaucoma (POAG) between swept-source optical coherence tomography (SS-OCT) and spectral-domain optical coherence tomography (SD-OCT) in myopic eyes.

Design: Prospective, case-control study

Methods: One hundred and fifty (150) myopic POAG eyes and 100 healthy myopic eyes underwent SD-OCT and SS-OCT in random order, on the same day. The locations of glaucomatous defect on SD-OCT thickness and deviation maps and SS-OCT wide-field thickness (thickness surface) and SuperPixel maps were rated, and the maps' accuracies were compared. The area under receiver operating characteristic (AUROC) of the peripapillary retinal nerve fiber layer (RNFL) and the macular parameters (GCL++: equivalent to ganglion cell-inner plexiform layer [GCIPL] + RNFL; GCL+: equivalent to GCIPL) from each of the devices for myopic POAG were calculated and compared.

Results: The wide-field RNFL thickness (thickness surface) map showed the best accuracy for glaucomatous defect in the inferotemporal (96.4%) and superotemporal (92.4%) regions. The RNFL/GCL++/GCL+ wide-field thickness (thickness surface) map showed better accuracy for glaucomatous defect in both the superotemporal and inferotemporal regions compared with the SD-OCT thickness map (all *P*s < 0.05). The average GCL++ (87.6%) and GCL+ (87.5%) thicknesses showed significantly greater AUROC for myopic POAG than did GCIPL thickness from SD-OCT (83.8%, all *P*s < 0.05).

Conclusions: In myopic eyes, the SS-OCT wide-field map exhibited better accuracy for glaucomatous defect and greater diagnostic power for POAG compared with the SD-OCT outcomes. This result might have been due to SS-OCT's wider scan and measurement area.

Diagnostic Accuracy of Wide-Field Map from Swept-Source Optical Coherence Tomography for Primary Open-Angle Glaucoma in Myopic Eyes

Yong Woo Kim[1], Jinho Lee[1,2], Jin-Soo Kim[3], and Ki Ho Park[1]

[1]Department of Ophthalmology, SeoulNationalUniversityHospital, SeoulNationalUniversityCollege of Medicine, Seoul, Korea

[2]Department of Ophthalmology, Hallym University Chuncheon Sacred Heart Hospital, Chuncheon, Korea

[3]Department of Ophthalmology, Chungnam National University Sejong Hospital, Sejong, Korea

Short Title:Diagnostic accuracy of SS-OCT wide-field map for myopic POAG

Word count: 3375

Corresponding Author:

Ki Ho Park, M.D., Ph.D.

Professor and Chairman

Department of Ophthalmology, SeoulNationalUniversityCollege of Medicine

101 Daehak-ro, Jongno-gu, Seoul03080, Korea

Phone: +82-2-2072-3172, Fax: +82-2-741-3187

E-mail: kihopark@snu.ac.kr

ABBREVIATIONS

AUROC: area under receiver operating characteristic, **AXL**: axial length, **BMO-MRW**: Bruch's membrane opening-minimum rim width, **CCT**: central corneal thickness, **FDR**: false discovery rate, **GCIPL**: ganglion cell-inner plexiform layer, **HVF**: Humphrey C 24-2 SITA-Standard visual field, **OCT**: optical coherence tomography, **POAG**: primary open-angle glaucoma, **RNFL**: retinal nerve fiber layer, **ROC**: receiver operating characteristic, **SD-OCT**: spectral-domain optical coherence tomography, **SNUH**: Seoul National University Hospital, **SS-OCT**: swept-source optical coherence tomography, **3D-NRT**: three-dimensional neuroretinal rim thickness, **VF**: visual field

INTRODUCTION

The prevalence of myopia is dramatically increasing in young generations, especially in East Asians, including Koreans.[1] The public concern for increasing myopia stems from the fact that it can lead to vision-threatening eye diseases such as retinal detachment, choroidal neovascularization, and glaucoma.[2] In particular, many epidemiological studies have indicated increased risk of primary open-angle glaucoma (POAG) in myopic eyes.[3,4] A systematic meta-analysis supported the idea that myopia increases the risk of POAG.[5]

Unfortunately, however, diagnosis and monitoring of POAG in myopic eyes are challenging.[6] Myopic eyes have divergent optic disc morphology such as tilted disc, peripapillary atrophy, and chorioretinal atrophy. These structural anomalies make accurate detection of glaucomatous optic disc changes difficult. In addition, vessel temporalization during axial elongation in myopic eyes alters the peak distribution of peripapillary retinal nerve fiber layer (RNFL) thickness and causes false-positives in optical coherence tomography (OCT) measurements.[7,8]

In response to the clinical demand for accurate diagnosis of POAG in myopic eyes, there have been many attempts to improve diagnostic power by using spectral-domain OCT (SD-OCT). The macular ganglion cell-inner plexiform layer (GCIPL) thickness and its asymmetrical difference across the horizontal raphe have shown improved diagnostic accuracy for POAG in highly myopic eyes.[9-11] Also, optic disc rim measurements such as Bruch's membrane opening-minimum rim width (BMO-MRW) from Spectralis OCT (Heidelberg Engineering, Inc., Heidelberg, Germany) or three-dimensional neuroretinal rim thickness (3D-NRT) from Cirrus HD-OCT (Carl Zeiss Meditec, Dublin, CA, USA) have exhibited greater diagnostic power for myopic POAG.[12,13]

Recently, swept-source OCT (SS-OCT, DRI OCT Triton, Topcon, Tokyo, Japan) has been proved effective for capturing of a wide 12×9 mm area in a single scan, thanks to its higher scanning speed and longer wavelength penetration relative to SD-OCT.[14] The wide-field map provided by SS-OCT is advantageous over conventional thickness and deviation maps from SD-OCT in that the macular and peripapillary structure can be evaluated simultaneously from a single scan. In this sense, our group reported a good diagnostic utility of the wide-field RNFL thickness map in detecting pre-perimetric and early-perimetric glaucoma eyes.[15,16]

The present study was initiated to confirm whether the wide-field map provided by SS-OCT is useful in detecting glaucomatous changes in myopic eyes. We evaluated the wide-field GCL++ (equivalent to RNFL+GCIPL from Cirrus HD-OCT) and GCL+ (equivalent to GCIPL in Cirrus HD-OCT) maps as well as the RNFL map and compared their accuracies for detection of glaucomatous structural defect relative to RNFL/GCIPL thickness and deviation maps from Cirrus HD-OCT. In addition, the diagnostic power for myopic POAG was compared among the measurement data from the two devices.

METHODS

The present study was a prospective case-control series study performed at Seoul National University Hospital (SNUH) after approval by the SNUH Institutional Review Board (IRB No.: H-1806-153-953). The participants in the study were patients enrolled consecutively from August 2018 who met the eligibility criteria. The study followed the tenets of the Declaration of Helsinki (1964), and written informed consent was obtained from each subject. The study protocol has been registered in the Clinical Research Information Service (CRIS) of the Korea Centers for Disease Control and Prevention (KCDC) (registration number: KCT0004980).

Study Subjects

For inclusion in the present study, subjects had to have myopia with refraction < –0.5 D or axial length (AXL) > 24 mm. High myopia was defined as refraction < –6.0 D or AXL > 26 mm. POAG was defined as including the presence of glaucomatous optic disc changes such as focal notching and thinning, RNFL defects on disc stereo photography and red-free fundus photography, glaucomatous visual field (VF) defect, and an open angle confirmed by gonioscopic examination. Glaucomatous VF defect was defined as (1) glaucoma hemifield test values outside the normal limits or (2) three or more abnormal points with a probability of being normal of $P< 5\%$, of which at least one point has a pattern deviation of $P< 1\%$, or (3) a pattern standard deviation of $P< 5\%$. The VF defects were confirmed on two consecutive reliable tests (fixation loss rate $\leq 20\%$, false-positive and false-negative error rates $\leq 25\%$).[17] Subjects were deemed to be healthy when no definite RNFL defect was found on red-free RNFL photography and they were found to be within normal limits on a glaucoma hemifield test of the standard automated perimetry.

The subjects initially underwent complete ophthalmic examinations including a medical history review, best-corrected visual acuity (BCVA), phakic status, refraction, slit-lamp biomicroscopy, Goldmann applanation tonometry, gonioscopy, dilated fundus examination, stereo optic-disc photography, red-free RNFL photography (VISUCAM, Carl Zeiss Meditec), and standard automated perimetry (HVF, Humphrey C 24-2 SITA-Standard visual field; Carl Zeiss Meditec). Also, the central corneal thickness (CCT) (Pocket II; Quantel Medical, Clermont-Ferrand, France) and AXL (AXIS-II Ultrasonic Biometer; Quantel Medical S.A., Bozeman, MT, USA) were measured.

The present study excluded subjects with a history of any ocular surgery such as glaucoma surgery, or a history of any retinal disease (e.g., diabetic retinopathy, uveitis, retinal vein occlusion, epiretinal membrane, or age-related macular degeneration). Eyes with ambiguous RNFL on red-free RNFL photography also were excluded. If both eyes were eligible for the present study, one eye was selected randomly.

SD-OCT and SS-OCT Imaging

The subjects underwent SD-OCT (Cirrus HD-OCT, Carl-Zeiss Meditec) and SS-OCT (DRI OCT Triton, Topcon) imaging in random order on the same day. All eyes were dilated (1% tropicamide, 2.5% phenylephrine) before undergoing OCT imaging. For Cirrus HD-OCT, a 200×200 macular cube scan and a 200×200 optic disc cube scan were obtained. The following macular GCIPL and peripapillary RNFL thicknesses were measured automatically by the built-in software (Cirrus HD-OCT Review Software, Ver. 10.0): average and sectoral (superotemporal, superior, superonasal, inferonasal, inferior, inferotemporal) measurements for GCIPL and average, sectoral (superior, nasal, inferior, and temporal) and 12 clock-hour measurements for RNFL thickness. For DRI OCT Triton, a 12×9 mm 3D Wide scan were obtained. The 3D Wide scan in DRI OCT Triton provides a 12×9 mm wide-field thickness map, a thickness surface map, and SuperPixel maps for the RNFL, GCL++ and GCL+ layers. The thickness surface map is displayed in 3D for selected layers (RNFL, GCL++, or GCL+) and can be rotated or zoomed-in and -out by mouse operation (**Figure 1**). The SuperPixel-200 map consists of 26×26 grids within a 5.2×5.2 mm^2 peripapillary area and 30×30 grids within a 6.0×6.0 mm^2 macular area, thereby providing a significance map based on the built-in normative database. The side length of each grid is 200 μm. The uncolored pixels indicate the normal range, whereas the yellow-colored or red-colored pixels indicate abnormality at P = 1%-5% and P< 1% of the normal level, respectively. The average, sectoral (superior, nasal, inferior, and temporal), and 12 clock-hour peripapillary RNFL thicknesses and average and sectoral (superotemporal, superior, superonasal, inferonasal, inferior, inferotemporal) GCL++ and GCL+ thicknesses were measured automatically by the built-in review program (IMAGEnet 6 Version 1.25, Topcon). All of the analyses were performed according to the right-eye orientation.

Additionally excluded from the present study were eyes with motion or blink artifacts (n = 14), defocus (n = 12), algorithm segmentation failure (n = 12), a signal strength < 6 (n = 16) or image quality < 30 (n = 3) on OCT scans, or any abnormalities (e.g., large peripapillary atrophy in the circumpapillary region that affected the scan circle where the OCT RNFL thickness measurement was obtained) (n = 4).

Definition of Glaucomatous Structural Defect

Detailed definitions of RNFL defect on red-free photography, Cirrus HD-OCT, and DRI OCT Triton have been provided elsewhere.[15,16] RNFL defects for red-free RNFL photography have been defined as diverging, arched or wedge-shaped, wider than the main retinal vessel at a distance of 1-disc diameter from the edge of the disc.

RNFL defect on the Cirrus HD-OCT thickness map was defined as a wedge-shaped dark-blue area surrounding an abrupt color-scale change. RNFL defect on the deviation map was defined as the presence of a wedge-shaped area of at least 20 contiguous yellow/red pixels along with RNFL thinning. On both maps, the width of the defect increased from the disc toward the edge of the map, and the minimum defect size was larger than the diameter of the major retinal vessel. GCIPL defects on the Cirrus HD-OCT thickness map were defined as

the presence of a blue/black region. For the deviation map, it was defined as the presence of an area coded in yellow/red, the size of which is greater than 10 pixels.

Defect on the DRI OCT Triton wide-field thickness map was defined as an arcuate or wedge-shaped diverging dark-blue (for RNFL and GCL+) or light-blue (for GCL++) area surrounding an abrupt color-scale change. The minimum defect size was larger than the diameter of a major retinal vessel. The wide-field thickness surface map was used to cross-check the three-dimensional (3D) thickness difference with the surrounding tissues. Defect on the SuperPixel-200 map was defined as the presence of a wedge-shaped area of at least 20 contiguous yellow/red pixels.

When RNFL defect on the red-free RNFL photography was not subsequently identified on the OCT maps, it was classified as a false-negative. If a defect on the OCT map did not match a defect on the red-free RNFL photography and/or HVF test results, it was classified as a false-positive. The inter-rater agreement for assessment of glaucomatous structural defect was obtained from three glaucoma specialists (YWK, JHL, and JSK) by estimation of Fleiss' kappa. If the readings did not match each other, they were determined by consensus of the three readers.

Data Analysis

Continuous variables were compared between the two groups by student t-test. Categorical variables were compared using a chi-square test. The accuracy for glaucomatous structural defect was measured according to the following equation: Accuracy = (true-positive + true-negative) / (true-positive + false-positive + true-negative + false-negative). McNemar's test was used to compare the sensitivity and specificity for detection of glaucomatous structural defect between the two OCT devices. The diagnostic performance of each parameter from the two OCT devices for the detection of myopic glaucoma was determined by calculating the area under receiver operating characteristic (AUROC) curve. The best cut-off value was selected according to the Youden index value (which maximizes the value of 'sensitivity + specificity – 1').[18] A receiver operating characteristic (ROC) analysis was performed using the "pROC" package in the open-platform R software.[19] The AUCs were compared using the "ROCtest" function in the "pROC" package, based on the method introduced by DeLong et al.[20] The false discovery rate (FDR) was controlled for using the Benjamini-Hochberg method. Except where stated otherwise, the data are presented as mean ± standard deviations, and the level of statistical significance was set at $P < 0.05$.

RESULTS

Subject Demographics

The present study enrolled 150 myopic glaucoma eyes and 100 healthy myopic eyes. The average age was 54.8 ± 12.8 years for myopic glaucoma and 51.8 ± 13.4 years for healthy myopic eyes (the controls), respectively (P = 0.11). There were no significant differences in age, gender, BCVA, phakic status, IOP, SE, disc area, AXL or CCT between the two groups (**Table 1**). The range of disc area was 1.03–3.55 mm^2 for myopic glaucoma and 1.04–3.22 mm^2 for healthy myopia. There was no difference in the microdisc proportion (disc area < 1.63 mm^2) between myopic glaucoma (n = 49, 32.7%) and healthy myopia (n = 27, 27%) (P = 0.42). The mean deviation (MD) of VF was –4.23 ± 5.68 dB for myopic glaucoma and 0.23 ± 1.83 dB for the healthy controls (P< 0.001). Among the myopic glaucoma eyes, 39 (26.0%) had RNFL defect in the inferotemporal region, 31 (20.7%) in the superotemporal region, and 80 (53.3%) in both the inferotemporal and superotemporal regions. The detailed demographic data are provided in **Table 1**.

Accuracy for Detection of Glaucomatous Defect

Three independent glaucoma specialists (Y.W.K, J.L, J.S.K) rated the presence of RNFL or GCIPL (GCL+/GCL++) defect from red-free RNFL photography, thickness and deviation maps from Cirrus HD-OCT and wide-field maps from DRI OCT Triton. The agreement attained was substantial to almost perfect (Fleiss Kappa 0.719 to 0.909) among the raters (**Table 2**).

Among the parameters, the wide-field RNFL thickness map showed the best accuracy for glaucomatous defect in the inferotemporal (96.4%) and superotemporal (92.4%) regions. For glaucomatous defect in the inferotemporal region, the SS-OCT wide-field RNFL thickness map showed better accuracy than the SD-OCT thickness map's (96.4 vs. 90.0%, adjusted P = 0.028). The wide-field GCL++ (96.4%) and GCL+ (95.9%) thickness maps also demonstrated better accuracy compared with the GCIPL thickness map from SD-OCT (78.5%, all adjusted Ps < 0.001). There were no significant differences between the RNFL deviation map and the wide-field RNFL SuperPixel map (adjusted P> 0.99), GCIPL deviation map and wide-field GCL++ SuperPixel map (adjusted P = 0.06) or GCL+ SuperPixel map (adjusted P = 0.92). For glaucomatous defect in the superotemporal region, the SS-OCT wide-field map was superior to the SD-OCT thickness or deviation map in the RNFL, GCL++, and GCL+ layers (**Table 3**).

The sensitivity, specificity, positive predictive value (PPV) and negative predictive value (NPV) for each map in detecting glaucomatous defect are provided in **Supplemental Table 1 (Supplemental Material at AJO.com)**. The wide-field RNFL thickness map showed better specificity for defect in the superotemporal region (98.0%) than did the RNFL thickness map from SD-OCT (71.7%, adjusted P< 0.001). The wide-field RNFL SuperPixel map also

showed better specificity for defect in the superotemporal region (87.0%) than did the RNFL deviation map from SD-OCT (69.0%, adjusted P = 0.016). The wide GCL++ and GCL+ thickness maps showed better specificity for defect in both the inferotemporal and superotemporal regions than did the GCIPL thickness map (all adjusted Ps < 0.001). The wide-field GCL++ SuperPixel map showed better specificity for defect in the inferotemporal region (88.0%) than did the GCIPL deviation map (72.0%, adjusted P = 0.027). However, the wide-field GCL+ SuperPixel map showed no statistically significant sensitivity or specificity differences relative to the GCIPL deviation map (**Supplemental Table 2, Supplemental Material at AJO.com**). Representative cases showing false-positivity and false-negativity in detection of glaucomatous defects are provided in **Figures 2** and **3**.

ROC Analysis

There was no significant AUROC difference for detection of myopic POAG between the average RNFL thicknesses from Cirrus HD-OCT and DRI OCT Triton (83.5 vs. 85.7%, adjusted P = 0.19). In the sectoral analysis, the superior and nasal quadrants showed marginally greater AUROC for DRI OCT Triton than for Cirrus HD-OCT (**Supplemental Table 3, Supplemental Material at AJO.com**). In the clock-hour analysis, the 1 o'clock (58.1 vs. 65.5%, adjusted P = 0.017) and 11 o'clock (71.9 vs. 76.7%, adjusted P = 0.017) sectors showed significantly greater AUROC for DRI OCT Triton than for Cirrus HD-OCT (**Figure 4, Supplemental Table 3, Supplemental Material at AJO.com**). Nevertheless, the 7 o'clock sector RNFL thickness from DRI OCT Triton showed the best diagnostic power for myopic POAG (AUC = 85.9%).

Macular GCL++ thickness (87.6%) and GCL+ thickness (87.5%) showed greater AUROC than did macular GCIPL thickness from Cirrus HD-OCT (83.8%, all adjusted Ps < 0.05). In the sectoral analysis, the macular GCL++ thicknesses in the inferonasal (81.3%) and inferior (87.5%) sectors showed greater AUROC compared with those in the corresponding sectors for GCIPL thickness (**Figure 4, Supplemental Table 4, Supplemental Material at AJO.com**). The macular GCL+ thickness in the superotemporal (82.8%), inferonasal (79.6%), inferior (86.3%), and inferotemporal (89.3%) sectors showed greater AUROC than did GCIPL thickness (**Figure 4, Supplemental Table 4, Supplemental Material at AJO.com**). Inferotemporal GCL+ thickness showed the best diagnostic power (AUC = 89.3%) for myopic POAG among the parameters.

DISCUSSION

The present study compared diagnostic accuracy for detection of glaucomatous structural defects in myopic eyes between wide-field thickness (thickness surface) and SuperPixel maps from SS-OCT (DRI OCT Triton) and conventional thickness and deviation maps from SD-OCT (Cirrus HD-OCT). In addition, the diagnostic power for POAG from the OCT measurement values were compared between the two devices for each of the peripapillary RNFL and macular ganglion cell layer parameters. Our data demonstrate the clinical utility of wide-field thickness/thickness surface and SuperPixel maps and their measurements for accurate diagnosis of myopic POAG.

The wide-field RNFL/GCL++/GCL+ thickness (thickness surface) maps showed significantly greater accuracy for detection of glaucomatous structural defects in both the superotemporal and inferotemporal regions compared with the conventional RNFL or GCIPL thickness maps from Cirrus HD-OCT. Especially, SS-OCT's specificity for glaucomatous defect was superior to that of SD-OCT. In terms of the SuperPixel maps, the accuracy was markedly superior to the RNFL and GCIPL deviation maps from Cirrus HD-OCT for glaucomatous defects in the superotemporal region, and showed comparable accuracy for defects in the inferotemporal region. Only the specificity of the GCL++ SuperPixel map for inferotemporal defects was significantly greater than that of the GCIPL deviation map from SD-OCT. Taken together, the SS-OCT (DRI OCT Triton) wide-field thickness and SuperPixel maps showed better accuracy for detection of glaucomatous defects in myopic eyes than did the conventional thickness and deviation maps from SD-OCT (Cirrus HD-OCT).

The significances of the present findings can be judged, tentatively, as follows. First, the wide-field thickness surface map enabled 3D evaluation of the peripapillary and macular structures of myopic eyes. Rather than simply distinguishing by color differences on the 2D thickness map, the wide-field thickness surface map, checking 3D thickness differences by rotating and zooming-in and –out, enabled accurate detection of myopic glaucomatous defects. Second, the wider OCT scan range of SS-OCT enabled accurate detection of glaucomatous defect. Conventional SD-OCT scans only a 6×6 mm^2 area of the peripapillary and macular regions, while SS-OCT scans a 12×9 mm^2 area at a time. The limited scan area of SD-OCT might limit its detection accuracy for glaucomatous defects relative to SS-OCT, especially for the superotemporal region of the macula. As the macula usually is located inferior to the optic disc, defects in the superior macular region continuing from superotemporal peripapillary RNFL defect may have been missed in the conventional macular scan from SD-OCT (6×6 mm^2 area, located inferior to the optic disc). Third, normative-database differences may have caused differences in accuracy between the SuperPixel map (SS-OCT) and the deviation map (SD-OCT) in the present study. Although Cirrus HD-OCT includes a large, healthy population of diverse races for its normative database, the average refraction of its study population was only –0.82 ± 1.96 D for peripapillary RNFL thickness and –1.0 ± 2.1 D for macular GCIPL thickness.[21,22] The low

proportion of myopia in the normative database is known to be associated with the so-called 'red disease' signs of myopia. To the best of our knowledge, detailed information on the normative database of the DRI OCT Triton has not yet been disclosed. Although still only speculative, the reason for the improved accuracy of the SuperPixel map for myopic POAG may be a possibly different proportion of myopia in DRI OCT Triton's normative database. Lastly, it might be argued that optic disc tilt and torsion may have influenced the results of the present study. There was no significant difference in the degree of optic disc torsion between myopic glaucoma (5.69 ± 19.0 degrees) and healthy myopic eyes (2.09 ± 16.2 degrees) (P = 0.11). There was a marginally significant difference in the degree of optic disc tilt between myopic glaucoma (disc ovality ratio, 1.19 ± 0.17) and healthy myopic eyes (disc ovality ratio, 1.14 ± 0.17) (P = 0.022). As there was no clinically meaningful difference in optic disc tilt and torsion between the case and controls, and as the effects of these factors on OCT measurements were the same between the two OCT devices, its impact on the present data seems minimal.

SS-OCT's AUROC for diagnosis of myopic POAG was significantly greater for peripapillary RNFL thicknesses in the 1 and 11 o'clock sectors and for average macular GCL++ and GCL+ thicknesses compared with SD-OCT's. Also, SS-OCT's GCL++ thickness in the inferonasal and inferior sectors as well as GCL+ thickness in the superotemporal, inferonasal, inferior, and inferotemporal sectors showed significantly greater diagnostic power than did SD-OCT's macular GCIPL thickness. GCL+ thickness in the inferotemporal sector showed the greatest diagnostic power for myopic POAG. Previous studies have reported that the measurement values between SD-OCT and SS-OCT are not interchangeable.[23,24] This is possibly due to the difference in the measurement regions between the two devices. The peripapillary RNFL measurement diameter is 3.4 mm for DRI OCT Triton and 3.46 mm for Cirrus HD-OCT. In SS-OCT, the RNFL thickness measurements close to the optic disc rim may have been beneficial for myopic eyes in that the effect of vessel temporalization therein may have been diminished. The measurement area of the macular parameter is within a 6 mm diameter circle for DRI OCT Triton and within a 4.8×4.0 mm elliptical annulus for Cirrus HD-OCT. A wider scan range in SS-OCT may be more advantageous for diagnosis of POAG in myopic eyes. Furthermore, the difference in the segmentation algorithms between the two OCT devices may influence the diagnostic power for myopic POAG.[25]

The present study has the following limitations. First, the percentages of high myopia cases in myopic POAG and healthy myopic eyes were 30.7 and 21.0, respectively. However, the present study also excluded a certain number of highly myopic eyes, which caused OCT scan defects such as poor segmentation error or defocus. This may have caused selection bias preventing our findings' extension and generalization to extremely high myopic eyes. Second, the present study investigated actual measurements and did not correct for the magnification effect with either device. And since we compared the results of uncorrected values from the two instruments, they would have been equally exposed to the magnification effect. In a hectic clinical setting, though, it can be more practical to use actual measurement values, in that correcting the data based on keratometry and AXL, for each and every patient, is prohibitively time-consuming.

In conclusion, the wide-field thickness (thickness surface) and SuperPixel maps from SS-OCT exhibited better accuracy and diagnostic power compared with the conventional maps from SD-OCT for detection of glaucomatous defects in myopic eyes. It is certainly worth taking advantage of this new technology for accurate diagnosis of POAG and prevention of unnecessary glaucoma treatment in healthy myopic eyes.

ACKNOWLEDGMENTS/DISCLOSURE

a. Funding/Support: None

b. Financial Disclosures: No financial disclosures.

c. Other Acknowledgments: Presented as Poster Theater at AAO 2019, San Francisco, CA, USA (PO163)

REFERENCES

1. Morgan IG, French AN, Ashby RS, et al. The epidemics of myopia: Aetiology and prevention. *Prog Retin Eye Res.*2018;62:134-149. doi:10.1016/j.preteyeres.2017.09.004
2. Ikuno Y. OVERVIEW OF THE COMPLICATIONS OF HIGH MYOPIA. *Retina.* 2017;37(12):2347-2351. doi:10.1097/IAE.0000000000001489
3. Suzuki Y, Iwase A, Araie M, et al. Risk factors for open-angle glaucoma in a Japanese population: the Tajimi Study. *Ophthalmology.* 2006;113(9):1613-1617. doi:10.1016/j.ophtha.2006.03.059
4. Kim KE, Kim MJ, Park KH, et al. Prevalence, Awareness, and Risk Factors of Primary Open-Angle Glaucoma: Korea National Health and Nutrition Examination Survey 2008-2011. *Ophthalmology.* 2016;123(3):532-541. doi:10.1016/j.ophtha.2015.11.004
5. Marcus MW, de Vries MM, Junoy Montolio FG, Jansonius NM. Myopia as a risk factor for open-angle glaucoma: a systematic review and meta-analysis. *Ophthalmology.* 2011;118(10):1989-1994.e1982.
6. Tan NYQ, Sng CCA, Jonas JB, Wong TY, Jansonius NM, Ang M. Glaucoma in myopia: diagnostic dilemmas. *Br J Ophthalmol.*2019;103(10):1347-1355. doi:10.1136/bjophthalmol-2018-313530
7. Hwang YH, Yoo C, Kim YY. Myopic optic disc tilt and the characteristics of peripapillary retinal nerve fiber layer thickness measured by spectral-domain optical coherence tomography. *J Glaucoma.* 2012;21(4):260-265. doi:10.1097/IJG.0b013e31820719e1
8. Leung CK, Yu M, Weinreb RN, et al. Retinal nerve fiber layer imaging with spectral-domain optical coherence tomography: interpreting the RNFL maps in healthy myopic eyes. *Invest Ophthalmol Vis Sci.* 2012;53(11):7194-7200. doi:10.1167/iovs.12-9726
9. Choi YJ, Jeoung JW, Park KH, Kim DM. Glaucoma detection ability of ganglion cell-inner plexiform layer thickness by spectral-domain optical coherence tomography in high myopia. *Invest Ophthalmol Vis Sci.* 2013;54(3):2296-2304. doi:10.1167/iovs.12-10530
10. Seol BR, Jeoung JW, Park KH. Glaucoma Detection Ability of Macular Ganglion Cell-Inner Plexiform Layer Thickness in Myopic Preperimetric Glaucoma. *Invest Ophthalmol Vis Sci.* 2015;56(13):8306-8313. doi:10.1167/iovs.15-18141
11. Kim YK, Yoo BW, Jeoung JW, Kim HC, Kim HJ, Park KH. Glaucoma-Diagnostic Ability of Ganglion Cell-Inner Plexiform Layer Thickness Difference Across Temporal Raphe in Highly Myopic Eyes. *Invest Ophthalmol Vis Sci.* 2016;57(14):5856-5863. doi:10.1167/iovs.16-20116
12. Malik R, Belliveau AC, Sharpe GP, Shuba LM, Chauhan BC, Nicolela MT. Diagnostic Accuracy of Optical Coherence Tomography and Scanning Laser Tomography for Identifying Glaucoma in Myopic Eyes. *Ophthalmology.* 2016;123(6):1181-1189. doi:10.1016/j.ophtha.2016.01.052
13. Kim YW, Park KH. Diagnostic Accuracy of Three-Dimensional Neuroretinal Rim Thickness for Differentiation of Myopic Glaucoma From Myopia. *Invest Ophthalmol Vis Sci.* 2018;59(8):3655-3666. doi:10.1167/iovs.18-24283

14. Hood DC, De Cuir N, Blumberg DM, et al. A Single Wide-Field OCT Protocol Can Provide Compelling Information for the Diagnosis of Early Glaucoma. *Transl Vis Sci Technol.* 2016;5(6):4. doi:10.1167/tvst.5.6.4

15. Lee WJ, Na KI, Kim YK, Jeoung JW, Park KH. Diagnostic Ability of Wide-field Retinal Nerve Fiber Layer Maps Using Swept-Source Optical Coherence Tomography for Detection of Preperimetric and Early Perimetric Glaucoma. *J Glaucoma.* 2017;26(6):577-585. doi:10.1097/IJG.0000000000000662

16. Lee WJ, Oh S, Kim YK, Jeoung JW, Park KH. Comparison of glaucoma-diagnostic ability between wide-field swept-source OCT retinal nerve fiber layer maps and spectral-domain OCT. *Eye (Lond).* 2018.

17. Anderson RD PV. Automated Static Perimetry. 2nd ed.St. Louis:Mosby, 1999.

18. Youden WJ. Index for rating diagnostic tests. *Cancer.* 1950;3(1):32-35. doi:10.1002/1097-0142(1950)3:1<32::AID-CNCR2820030106>3.0.CO;2-3

19. Robin X, Turck N, Hainard A, et al. pROC: an open-source package for R and S+ to analyze and compare ROC curves. *BMC Bioinformatics.* 2011;12:77. doi:10.1186/1471-2105-12-77

20. DeLong ER, DeLong DM, Clarke-Pearson DL. Comparing the areas under two or more correlated receiver operating characteristic curves: a nonparametric approach. *Biometrics.* 1988;44(3):837-845. doi:10.2307/2531595

21. Mwanza JC, Durbin MK, Budenz DL, et al. Profile and predictors of normal ganglion cell-inner plexiform layer thickness measured with frequency-domain optical coherence tomography. *Invest Ophthalmol Vis Sci.* 2011;52(11):7872-7879. doi:10.1167/iovs.11-7896

22. Knight OJ, Girkin CA, Budenz DL, Durbin MK, Feuer WJ, Cirrus OCTNDSG. Effect of race, age, and axial length on optic nerve head parameters and retinal nerve fiber layer thickness measured by Cirrus HD-OCT. *Arch Ophthalmol.*2012;130(3):312-318. doi:10.1001/archopthalmol.2011.1576

23. Ha A, Lee SH, Lee EJ, Kim TW. Retinal Nerve Fiber Layer Thickness Measurement Comparison Using Spectral Domain and Swept Source Optical Coherence Tomography. *Korean J Ophthalmol.*2016;30(2):140-147. doi:10.3341/kjo.2016.30.2.140

24. Lee SY, Bae HW, Kwon HJ, Seong GJ, Kim CY. Repeatability and Agreement of Swept Source and Spectral Domain Optical Coherence Tomography Evaluations of Thickness Sectors in Normal Eyes. *J Glaucoma.* 2017;26(2):e46-e53. doi:10.1097/IJG.0000000000000536

25. Pierro L, Gagliardi M, Iuliano L, Ambrosi A, Bandello F. Retinal nerve fiber layer thickness reproducibility using seven different OCT instruments. *Invest Ophthalmol Vis Sci.* 2012;53(9):5912-5920. doi:10.1167/iovs.11-8644

LEGENDS

Figure 1. Wide-Field Map Provided by DRI OCT Triton

Representative Atlas of wide-field map of retinal nerve fiber layer (RNFL, A–D), GCL++ (RNFL + ganglion cell-inner plexiform layer [GCIPL], E–H), and GCL+ (GCIPL, I–L) provided by DRI OCT Triton for right eye of 52-year-old male with primary open-angle glaucoma (POAG). The wide-field map can be featured in the thickness map (A, E, I) and thickness surface map (B, F, J), which are provided in a three-dimensional (3D) manner and can be zoomed-in and -out (C, G, K), and SuperPixel maps (D, H, L). (M) Red-free RNFL photography captured by DRI OCT Triton. (N) Combined SuperPixel map of RNFL and GCL++ (D+H). (O) Combined SuperPixel map of RNFL and GCL+ (D+L).

Figure 2. False-Positive Red Signs of Cirrus HD-OCT in Healthy Myopia

Left eye of 41-year-old female with highly myopic refraction (spherical equivalence = –11.25 D). Red-free retinal nerve fiber layer (RNFL) photography (light-blue box) showed no definite RNFL defects. Cirrus HD-OCT (yellow box) reported red signs in the inferior peripapillary and macular regions. DRI OCT Triton wide-field maps (dark-red box), however, showed no abnormalities.

Figure 3. False-Negative Signs of Cirrus HD-OCT in Myopic Eyes with Primary Open-Angle Glaucoma

Right eye of 63-year-old female with primary open-angle glaucoma. Her refraction was –4.5 D, and the axial length was 24.29 mm. Red-free retinal nerve fiber layer (RNFL) photography (light-blue box) showed a wedge-shaped RNFL defect in the superotemporal area. Cirrus HD-OCT (yellow box), however, reported green signs for both peripapillary RNFL and macular ganglion cell-inner plexiform layer (GCIPL) thicknesses. The RNFL thickness map revealed only a slit-like RNFL defect in the superotemporal area, while the GCIPL maps did not detect any defects. The wide-field RNFL thickness and thickness surface maps from DRI OCT Triton (dark-red box) demonstrated an obvious wedge-shaped RNFL defect in the superotemporal area.

Figure 4. Diagnostic Power of RNFL, GCL++, and GCL+ Thickness from DRI OCT Triton

Comparison of diagnostic power between sectoral measurements of DRI OCT Triton (RNFL/GCL++/GCL+ thicknesses) and Cirrus HD-OCT (RNFL and GCIPL thicknesses) are schematized. The sectoral region where DRI OCT Triton measurement is significantly superior to that of Cirrus HD-OCT is shaded in light green. The sectoral region with the greatest diagnostic power (i.e., greatest area under receiver operating characteristic [AUROC]

curve) is shaded in pink. In the clock-hour analysis, the 1 o'clock (58.1 vs. 65.5%, adjusted *P* = 0.017) and 11 o'clock (71.9 vs. 76.7%, adjusted *P* = 0.017) sectors showed significantly greater AUROC for DRI OCT Triton than for Cirrus HD-OCT. Nevertheless, the 7 o'clock sector RNFL thickness from DRI OCT Triton showed the best diagnostic power for myopic POAG (AUC = 85.9%).

Macular GCL++ thickness (87.6%) and GCL+ thickness (87.5%) showed greater AUROC than did macular GCIPL thickness from Cirrus HD-OCT (83.8%, all adjusted *P*s < 0.05). In the sectoral analysis, the macular GCL++ thicknesses in the inferonasal (81.3%) and inferior (87.5%) sectors showed greater AUROC compared with those in the corresponding sectors for GCIPL thickness. The macular GCL+ thickness in the superotemporal (82.8%), inferonasal (79.6%), inferior (86.3%), and inferotemporal (89.3%) sectors showed greater AUROC than did GCIPL thickness. Inferotemporal GCL++ (88.0%) and GCL+ thickness (89.3%) showed the greatest AUROC. Detailed information is provided in **Supplemental Tables 3 and 4(Supplemental Material at AJO.com).**

Table 1. Subject Demographics

	Myopic POAG (n = 150)	**Healthy Myopia (n = 100)**	***P*-value**
Age, yr	54.8 ± 12.8	51.8 ± 13.4	0.11[a]
Gender, female, *n* (%)	65 (43.3)	52 (52.0)	0.27[b]
BCVA, logMAR	0.04 ± 0.12	0.02 ± 0.12	0.37
Phakia, *n* (%)	139 (92.7)	95 (95.0)	
IOP, mmHg	13.3 ± 2.7	13.6 ± 2.6	0.44[a]
SE, *D*	–3.78 ± 3.07	–3.14 ± 2.66	0.13[a]
AXL, mm	25.26 ± 1.17	24.89 ± 1.21	0.09[a]
High myopia, *n* (%)	46 (30.7)	21 (21.0)	0.12[b]
CCT, µm	546.6 ± 36.6	544.5 ± 37.2	0.68[a]
RNFL thickness, µm	**73.5 ± 10.8**	**87.3 ± 9.6**	**<0.001**[a]
Rim area, mm^2	**0.84 ± 0.23**	**1.12 ± 0.23**	**<0.001**[a]
Disc area, mm^2	1.89 ± 0.51	1.91 ± 0.41	0.68[a]
Average C/D	**0.72 ± 0.12**	**0.61 ± 0.15**	**<0.001**[a]
Vertical C/D	**0.73 ± 0.12**	**0.57 ± 0.15**	**<0.001**[a]
Cup volume, mm^3	**0.425 ± 0.281**	**0.284 ± 0.222**	**<0.001**[a]
Average GCIPL thickness, µm	**69.6 ± 8.4**	**79.9 ± 6.3**	**<0.001**[a]
Minimum GCIPL thickness, µm	**59.9 ± 11.7**	**75.3 ± 11.4**	**<0.001**[a]
MD. dB	**–4.23 ± 5.68**	**0.23 ± 1.83**	**<0.001**[a]
PSD, dB	**5.94 ± 4.52**	**1.84 ± 1.03**	**<0.001**[a]
VFI, %	**87.1 ± 16.5**	**98.9 ± 2.2**	**<0.001**[a]

Mean ± standard deviation. [a] Comparison was performed using student t-test; [b] Comparison was performed using chi-square test. Statistically significant *P*-values are shown in bold.

POAG: primary open-angle glaucoma, BCVA: best corrected visual acuity, logMAR: logarithm of the minimum angle of resolution, IOP: intraocular pressure, SE: spherical equivalence, AXL: axial length, RNFL: retinal nerve fiber layer, C/D: cup-to-disc ratio, GCIPL: ganglion cell-inner plexiform layer, MD: mean deviation of visual field, PSD: pattern standard deviation of visual field, VFI: visual field index

Table 2. Inter-rater Agreement for Detection of Glaucomatous Defect

	Fleiss Kappa	Strength of agreement
RNFL photo	0.861	Almost perfect
RNFL thickness map	0.719	Substantial
RNFL deviation map	0.810	Almost perfect
GCIPL thickness map	0.763	Substantial
GCIPL deviation map	0.815	Almost perfect
Wide RNFL thickness map	0.847	Almost perfect
Wide RNFL SuperPixel map	0.909	Almost perfect
Wide GCL++ thickness map	0.723	Substantial
Wide GCL++ SuperPixel map	0.861	Almost perfect
Wide GCL+ thickness map	0.754	Substantial
Wide GCL+ SuperPixel map	0.772	Substantial

RNFL: retinal nerve fiber layer, GCIPL: ganglion cell-inner plexiform layer, GCL++: RNFL+GCIPL, GCL+: GCIPL

Table 3. Comparison of Accuracy for Glaucomatous Defect between SS-OCT and SD-OCT

	Inferotemporal defect		Superotemporal defect	
	Accuracy	***P*-value** [a]	**Accuracy**	***P*-value** [a]
RNFL thickness map (SD-OCT)	**90.0**	**0.028**	**79.9**	**<0.001**
Wide RNFL thickness map (SS-OCT)	**96.4**		**92.4**	
RNFL deviation map (SD-OCT)	90.0	>0.99	**71.1**	**0.016**
Wide RNFL SuperPixel map (SS-OCT)	91.0		**82.4**	
GCIPL thickness map (SD-OCT)	**78.5**	**<0.001**	**71.1**	**<0.001**
Wide GCL++ thickness map (SS-OCT)	**96.4**		**90.1**	
GCIPL thickness map (SD-OCT)	**78.5**	**<0.001**	**71.1**	**<0.001**
Wide GCL+ thickness map (SS-OCT)	**95.9**		**88.2**	
GCIPL deviation map (SD-OCT)	86.8	0.06	**74.4**	**0.016**
Wide GCL++ SuperPixel map (SS-OCT)	93.2		**84.4**	
GCIPL deviation map (SD-OCT)	86.8	0.92	**74.4**	**0.016**
Wide GCL+ SuperPixel map (SS-OCT)	88.1		**84.4**	

[a] *P*-values adjusted by Benjamini-Hochberg method to compensate for multiple comparison.

SS-OCT: swept-source optical coherence tomography, SD-OCT: spectral-domain optical coherence tomography, RNFL: retinal nerve fiber layer, GCIPL: ganglion cell-inner plexiform layer, GCL++: RNFL+GCIPL, GCL+: GCIPL

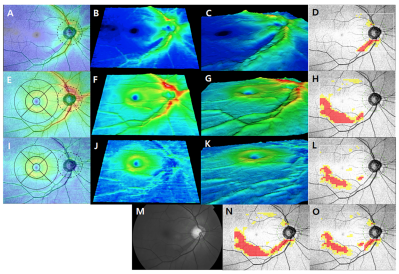

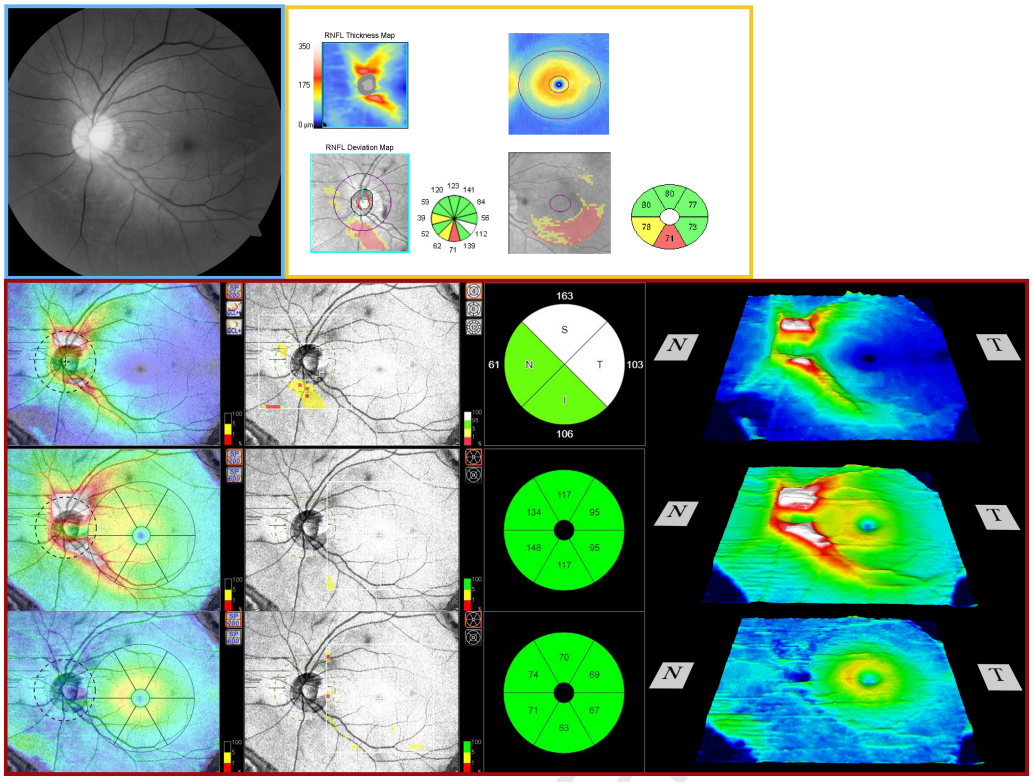

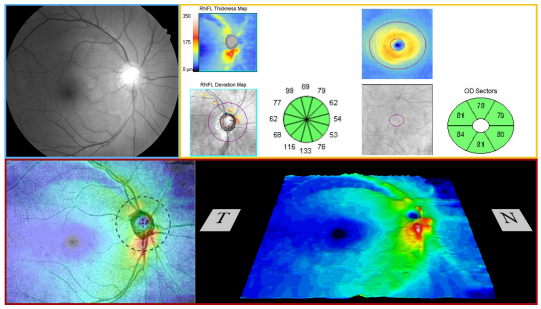

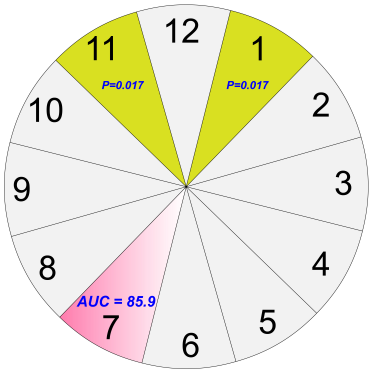

RNFL thickness
vs. Cirrus HD-OCT

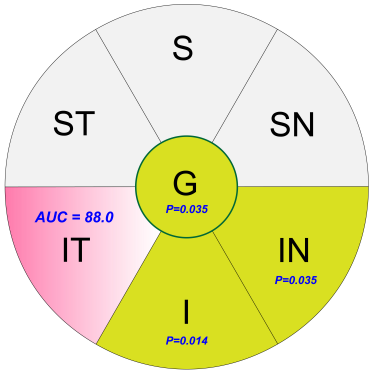

GCL++ thickness
vs. GCIPL thickness

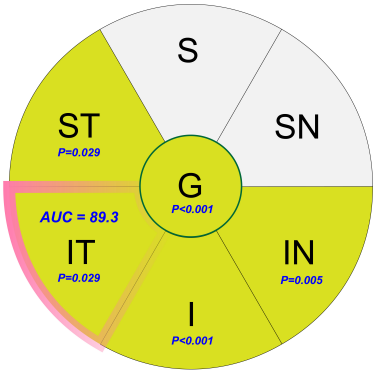

GCL+ thickness
vs. GCIPL thickness

BIOSKETCH

Dr. Yong Woo Kim is a research assistant professor in the Department of Ophthalmology at Seoul National University Hospital (SNUH), Seoul, Korea. Dr. Kim received his MD from Seoul National University College of Medicine in 2009 and finished his Ophthalmology residency and Glaucoma fellowship at SNUH. His current research interest includes optic nerve head imaging, diagnosis and monitoring of glaucoma, and glaucoma genomics.

TABLE OF CONTENTS STATEMENT

The wide-field maps from swept-source optical coherence tomography (OCT) had better accuracy for glaucomatous defect and greater diagnostic power for primary open-angle glaucoma compared with the conventional maps from spectral-domain OCT in myopic eyes.